

## **Enstatite, $\text{Mg}_2\text{Si}_2\text{O}_6$ : A neutron diffraction refinement of the crystal structure and a rigid-body analysis of the thermal vibration**

Subrata Ghose

Department of Geological Sciences, University of Washington,  
Seattle, Washington 98195, USA

Verner Schomaker

Department of Chemistry, University of Washington, Seattle, Washington 98195, USA

and R. K. McMullan

Chemistry Department, Brookhaven National Laboratory, Upton, New York 11973,  
USA

Received: November 20, 1984

### ***Enstatite / Crystal structure / Neutron diffraction / Rigid-body analysis***

**Abstract.** Synthetic enstatite,  $\text{Mg}_2\text{Si}_2\text{O}_6$ , is orthorhombic, space group *Pbca*, with eight formula units per cell and lattice parameters  $a = 18.235(3)$ ,  $b = 8.818(1)$ ,  $c = 5.179(1)$  Å at 23°C. A least-squares structure refinement based on 1790 neutron intensity data converged with an agreement factor  $R(F^2) = 0.032$ , yielding Mg–O and Si–O bond lengths with standard deviations of 0.0007 and 0.0008 Å, respectively. The variations observed in the Si–O bond lengths within the silicate tetrahedra *A* and *B* are caused by the differences in primary coordination of the oxygen atoms and the proximity of the magnesium ions to the silicon atoms. The latter effect is most pronounced for the bridging bonds of tetrahedron *A*. The smallest O–Si–O angle is the result of edge-sharing by the Mg(2) octahedron and the *A* tetrahedron. An analysis of rigid-body thermal vibrations of the two crystallographically independent  $[\text{SiO}_4]$  tetrahedra indicates considerable librational motion, leading to a thermal correction of apparent Si–O bond lengths as large as +0.002 Å at room temperature.

## Introduction

Enstatite is the magnesium end-member  $\text{Mg}_2\text{Si}_2\text{O}_6$  of orthopyroxenes  $(\text{Mg,Fe})_2\text{Si}_2\text{O}_6$ . It is a rock-forming silicate occurring in terrestrial and lunar rocks and meteorites and is considered to be an important constituent of the earth's upper mantle. Because of its geophysical importance, we have chosen it for detailed structural and lattice dynamical studies on the effects of pressure and temperature on pyroxene minerals. The enstatite structure has been refined by a number of workers using X-ray diffraction data measured under ambient laboratory pressure and temperature (Morimoto and Koto, 1969; Ghose and Wan, 1976; Hawthorne and Ito, 1977; Ghose, Wan, Ralph and McMullan, 1980; Sasaki, Fujino, Takéuchi and Sadanaga, 1980; Sasaki, Takéuchi, Fujino and Akimoto, 1982; Ohashi, 1984), as well as at 21 kbar (Ghose, et al., 1980) and (on  $\text{Mg}_{0.3}\text{Fe}_{0.7}\text{SiO}_3$ ) up to  $850^\circ\text{C}$  (Smyth, 1973). We present here the results of a neutron diffraction study under ambient conditions, undertaken to obtain accurate positional and thermal vibration parameters that are unbiased by aspherical bonding electron densities of the atoms. We also present an analysis of the configurational differences in the silicate and magnesium polyhedra, together with an analysis of the rigid-body motion of the individual silicate tetrahedra of the single silicate chains. Neutron studies on two other pyroxenes, diopside,  $\text{CaMgSi}_2\text{O}_6$ , and spodumene,  $\text{LiAlSi}_2\text{O}_6$ , have been completed (Ghose and Busing, 1984).

## Experimental

Crystals of orthoenstatite,  $\text{Mg}_2\text{Si}_2\text{O}_6$ , were obtained by the primary crystallization in the system  $\text{MgO} - \text{SiO}_2 - \text{lithium vanadomolybdate}$  (Ito, 1975). Slow cooling ( $\sim 1.5$  deg/h) of the melt from  $930^\circ\text{C}$  to  $650^\circ\text{C}$  yielded prismatic crystals with [001] elongation, exhibiting forms {100}, {210}, and {011}. The reported composition is essentially  $\text{MgSiO}_3$ , with 0.17 wt%  $\text{Li}_2\text{O}$  and 0.27 wt%  $\text{V}_2\text{O}_5$ . The crystal selected for study (Table 1) was mounted within a few degrees of the  $c$  axis. Diffraction data were collected at room temperature on a 4-circle diffractometer at the Brookhaven High Flux Beam Reactor. The neutron beam, monochromatized by reflection from the 002 planes of a beryllium crystal, was of wavelength  $1.0024(1)$  Å based on KBr ( $a_0 = 6.6000$  Å at  $25^\circ\text{C}$ ).

The unit-cell parameters (Table 1) were determined by a least-squares fit of  $\sin^2\theta$  values for 32 reflections distributed over the reciprocal lattice in the range  $45^\circ < 2\theta < 57^\circ$ . Intensity data were recorded for reflections  $(+h, +k, +l; \sin\theta/\lambda \leq 0.80 \text{ \AA}^{-1})$  using  $\theta/2\theta$  step scans over scan ranges  $\Delta(2\theta) = 3.0^\circ$  for  $0^\circ < 2\theta < 65^\circ$  and  $\Delta(2\theta) = 2.38 + 2.52 \tan\theta$ , for  $65^\circ < 2\theta < 107^\circ$ . Between 60 and 88 points were sampled on the scan profiles, with counting time at each point ( $\sim 2$  s) being determined by a fixed

**Table 1.** Crystal data and structure refinement.

A. Crystal sample		
synthetic enstatite: Mg <sub>2</sub> Si <sub>2</sub> O <sub>6</sub> <sup>a</sup>		
principal faces	{100}, {210}, {011}	
maximum dimensions (mm)	1.30 × 1.00 × 2.40	
volume (mm <sup>3</sup> )	2.50	
D <sub>c</sub> (g · cm <sup>-3</sup> )	3.204	
abs. coeff. (μ cm <sup>-1</sup> )	2.40 × 10 <sup>-3</sup>	
B. Crystal data		
space group	<i>Pbca</i>	
cell content	8[Mg <sub>2</sub> Si <sub>2</sub> O <sub>6</sub> ]	
unit-cell parameters (23 °C)		
<i>a</i> (Å)	18.235(3)	
<i>b</i> (Å)	8.818(1)	
<i>c</i> (Å)	5.179(1)	
<i>V</i> (Å <sup>3</sup> )	832.8(4)	
C. Structure refinement		
	extinction model <sup>b</sup>	
	isotropic	anisotropic
no. of observations ( <i>N<sub>O</sub></i> )	1790	1790
no. of parameters ( <i>N<sub>P</sub></i> )	92	97
indices of fit <sup>c</sup>		
<i>R</i> ( <i>F</i> <sup>2</sup> )	0.036	0.032
<i>wR</i> ( <i>F</i> <sup>2</sup> )	0.043	0.039
<i>S</i>	1.18	1.08
scale factor, <i>k</i>	3.112(5)	3.111(5)
extinction parameters (rad <sup>-1</sup> × 10 <sup>-5</sup> )		
<i>g</i> <sub>11</sub> ( <i>g</i> <sub>iso</sub> ), <i>g</i> <sub>22</sub> , <i>g</i> <sub>33</sub>	14.8(2)	8.1(8), 4.5(4), 4.4(1)
<i>g</i> <sub>12</sub> , <i>g</i> <sub>13</sub> , <i>g</i> <sub>23</sub>		2.7(7), -0.3(4), 1.4(3)

<sup>a</sup> Ito (1975).<sup>b</sup> Type I crystal with Lorentzian distribution of mosaicity (Becker and Coppens, 1974).<sup>c</sup>  $R(F^2) = \Sigma \Delta / \Delta F_o^2$ ;  $wR(F^2) = \{\Sigma w \Delta^2 / \Sigma F_o^4\}^{\frac{1}{2}}$ ;  $S = \{\Sigma w \Delta^2 / N_o - N_p\}^{\frac{1}{2}}$ , where  $\Delta = |F_o^2 - F_c^2|$ .

count in the direct-beam monitor. The intensities of two reflections were remeasured at 3 h intervals and were found to be constant within 2% during the course of the experiment. For each reflection, the integrated intensity *I* was obtained by subtracting the background *B* as estimated from the first and last tenth parts of the total scan. The variance in intensity was derived from counting statistics. Absorption corrections were calculated (de Meulenaer and Tompa, 1965; Templeton and Templeton, 1973) from the measured crystal dimensions and the linear absorption coefficient  $\mu$  based on the tabulated neutron ( $\mu/\rho$ ) values of the International Tables for X-ray Crystallography (Vol. III, 1962). Multiple observations were averaged to give squared structure factors  $F_o^2 (= I \cdot$

$\sin 2\theta$ ) for 1790 independent reflections, all of which were included in the refinement. None of the  $F_o^2$  values was significantly less than zero.

Full-matrix least-squares refinement of the structure was carried out with a modified version of the computer program of Busing, Martin and Levy (1962). The quantity minimized was  $\sum w|F_o^2 - F_c^2|^2$  with weights  $w = [\sigma_c^2(F_o^2) + (0.01 F_o^2)^2]^{-1}$ , where  $\sigma_c^2(F_o^2)$  is the variance from counting statistics. Neutron scattering lengths (fm), 5.380 for magnesium, 4.1491 for silicon, and 5.803 for oxygen, were taken from Koester (1977). Starting atomic positional and anisotropic thermal parameters were those determined by Ghose and Wan (1976). In the final refinement stage, secondary extinction factors (Becker and Coppens, 1974) were included as variable parameters, and refinements were carried to convergence for both isotropic and anisotropic extinction models, giving the indices of fit listed in Table 1. The latter model was taken as the better description of extinction in the crystal on the basis of Hamilton's (1964)  $R$ -factor ratio test at the 99.5% confidence level. The final atomic parameters in Table 2 are from that refinement. The maximum differences  $|\Delta/\sigma|$  between the two refinements were only 0.48 and 1.92 in positional and displacement parameters, respectively. However, the  $U_{33}$  values were systematically greater, and the  $U_{11}$  and  $U_{22}$  values less, in the anisotropic refinement than in the isotropic. The extinction corrections were large: 35 reflections had correction factors ( $\times F_o^2$ ) less than 0.75, the most severe being 0.35 for reflection 060. In the final difference map, the largest residual densities  $|\Delta\rho|$  were randomly distributed and were  $\sim 1.3\%$  of  $\rho$  at oxygen sites in the  $F_o$  synthesis. Lists of structure factors corrected for extinction were deposited<sup>1</sup>.

## Results and discussion

The crystal structure is illustrated in Figure 1, the crystallographically independent silicate chains  $A$  and  $B$ , and magnesium octahedra Mg(1) and Mg(2) in Figure 2, octahedral chains in Figure 3 and oxygen coordinations in Figure 4. The atomic notation is that of Burnham's (1967). The positional parameters in Table 2 differ very little ( $\leq 2.1\sigma$ ) from those determined by X-ray diffraction for this synthetic enstatite (Sasaki et al., 1982), but there were significant differences in the  $U_{ij}$ 's ( $5.5\sigma$  or 16%). The internuclear distances and angles relevant to this discussion are given in Table 3 and Figure 4; the standard deviations estimated from the final variance-covariance matrix are 0.0008 Å and 0.0007 Å for the Si–O and Mg–O bond lengths, respectively. Thermal motion corrections to the Si–O bond lengths up to a maximum of 0.0034 Å are estimated from an analysis (vide

<sup>1</sup> Additional material to this paper can be ordered from the Fachinformationszentrum Energie-Physik-Mathematik, D-7514 Eggenstein-Leopoldshafen 2, FRG. Please quote reference no. CSD 51 555, the names of the authors and the title of the paper.

**Table 2.** Atomic parameters<sup>a</sup> and standard errors, in parentheses, both  $\times 10^5$ , for enstatite.

Atom	<i>x</i>	<i>y</i>	<i>z</i>	<i>U</i> <sub>11</sub>	<i>U</i> <sub>22</sub>	<i>U</i> <sub>33</sub>	<i>U</i> <sub>12</sub>	<i>U</i> <sub>13</sub>	<i>U</i> <sub>23</sub>
Mg(1)	37584(3)	65393(5)	86580(10)	609(17)	454(17)	371(19)	−32(15)	−57(14)	11(15)
Mg(2)	37681(3)	48693(6)	35882(10)	817(19)	664(19)	526(20)	−69(16)	−186(16)	49(16)
Si(A)	27167(3)	34166(7)	5031(12)	378(21)	373(23)	271(23)	−54(18)	34(18)	−13(20)
Si(B)	47357(3)	33732(7)	79827(12)	385(22)	321(21)	301(22)	34(18)	−22(18)	23(19)
O(1A)	18346(2)	34009(5)	3471(9)	377(16)	551(17)	488(18)	−18(13)	12(13)	19(14)
O(1B)	56231(2)	34034(5)	80017(9)	424(16)	563(16)	451(17)	6(13)	−21(14)	29(14)
O(2A)	31091(3)	50255(5)	4319(9)	732(18)	480(17)	563(19)	−207(14)	−106(15)	64(14)
O(2B)	43277(3)	48289(5)	68909(10)	737(17)	514(16)	490(18)	235(13)	−112(15)	28(15)
O(3A)	30318(3)	22259(5)	−16799(9)	560(16)	746(18)	426(18)	55(14)	−40(15)	−197(14)
O(3B)	44762(3)	19506(5)	60361(9)	579(16)	623(17)	431(16)	−74(14)	52(14)	−144(13)

<sup>a</sup> Anisotropic thermal parameters are of the form:  $\exp[-2\pi^2(a^{*2}U_{11}h^2 + b^{*2}U_{22}k^2 + \dots 2b^*c^*U_{23}kl)]$ .

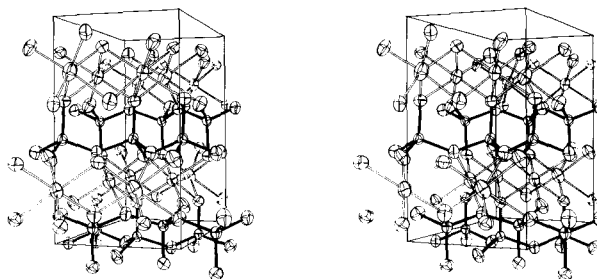


**Fig. 1.** The structure of enstatite in a stereoscopic view with  $a$  vertical  $b$  forward left. One-half of the cell ( $0 \leq x \leq \frac{1}{2}$ ) is outlined. The thermal ellipsoids enclose 99.9% probability surfaces (Johnson, 1976). Shown here are two  $(\text{SiO}_3)_n$  chains of each type,  $A$  and  $B$ , extending along  $[001]$  and located near  $x = \frac{1}{2}$  and  $x = 0$ , respectively. In both chains, the bridging  $\text{O}(3)$  and terminal  $\text{O}(2)$  atoms lie roughly in the  $[100]$  planes with the  $\text{Si}-\text{O}(1)$  bonds approximately parallel to  $[100]$ . The  $\text{Mg}$  atoms between chains  $A$  and  $B$  occupy octahedral sites in  $(\text{Mg}_2\text{O}_6)_n$  ribbons extending along  $[001]$ .

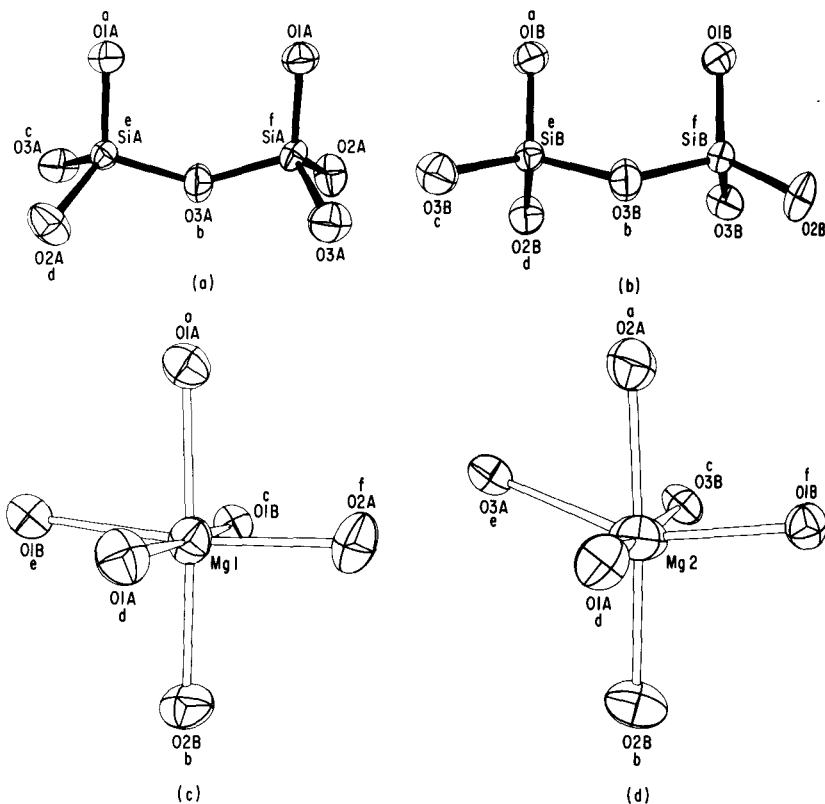


**Fig. 2.** The silicate chains  $A$  and  $B$  and magnesium octahedra  $\text{Mg}(1)$  and  $\text{Mg}(2)$ . Lower case letters above and below the atom labels refer to symmetry operations given in Table 3. In both silicate chains, the  $[\text{Si}-\text{O}(3)-\text{Si}]$  bridges lie on the plane of the paper.

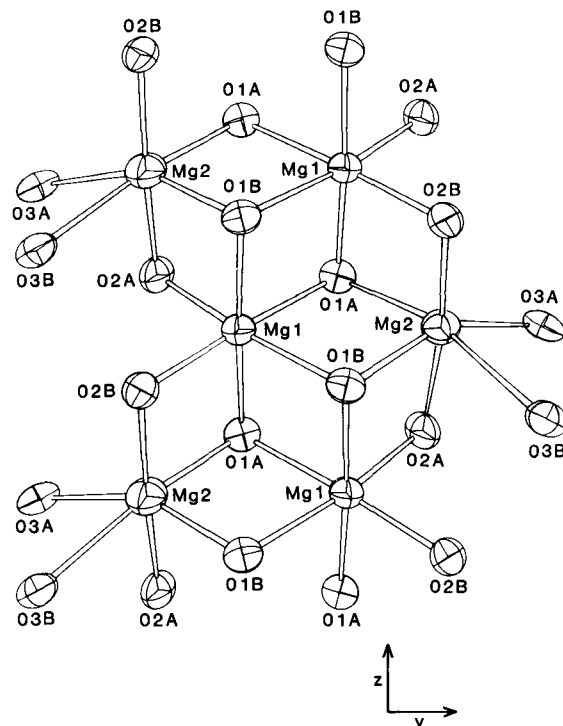


Fig. 3. Double chain of edge-sharing octahedra  $[\text{Mg}(1)\text{O}_6]$  and  $[\text{Mg}(2)\text{O}_6]$  parallel to  $[001]$ .

infra) of the nuclear vibration tensors  $U_{ij}$  in Table 2. The precision of the present structure determination allows a more detailed description of the bonding geometry in enstatite than has hitherto appeared in the literature.

### The silicate chains

The two  $[\text{SiO}_4]$  tetrahedra *A* and *B* each form a distinct chain along the *c* axis by sharing oxygen atoms O(3). Of the two tetrahedra, *B* is larger, and, as a consequence, the *A* chains are more extended than the *B* chains<sup>2</sup>. The shortest  $\text{Si} \cdots \text{Si}$  vectors in the *A* and *B* chains are of lengths 3.053(1) Å and 3.013(1) Å, respectively, and subtend angles of 116.05(3)° and 118.52(3)°. Corresponding  $\text{O}(3) \cdots \text{O}(3)$  distances are 2.634(1) Å and 2.765(1) Å, with the subtended angles being 158.85(3)° and 138.97(3)°.

In both chains, the bridging  $\text{Si}-\text{O}(3)$  bonds are the longest of three types,  $\text{Si}-\text{O}(1)$ ,  $\text{Si}-\text{O}(2)$ ,  $\text{Si}-\text{O}(3)$ , and vary the most i.e., from

<sup>2</sup> The extension (or kinking) of a single silicate chain is measured by the  $\text{O}(3)-\text{O}(3')-\text{O}(3)''$  angle; for a fully extended chain, this angle is 180°.

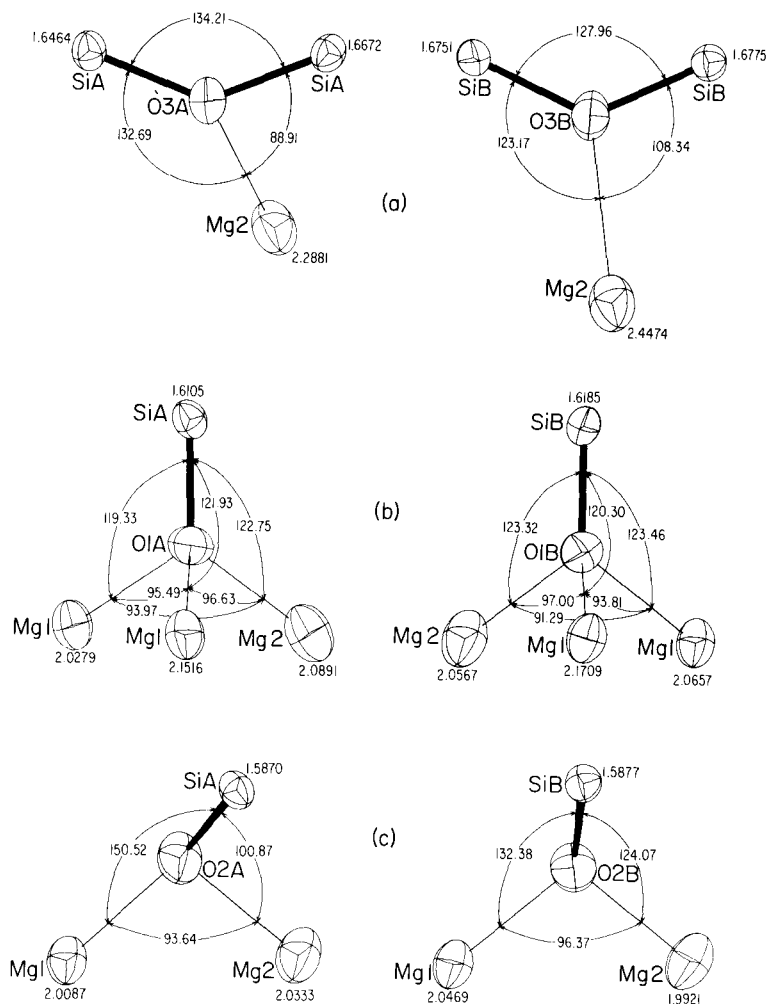


**Fig. 4.** The oxygen coordinations shown in order of decreasing Si–O bond lengths.

1.6464(8) Å to 1.6775(8) Å. The [Si–O(3)–Si] group of chain *A* is notably asymmetric, with bond length difference  $\Delta(\text{Si–O}) = 0.021(1)$  Å, in contrast to the marginal difference, 0.002(1) Å in chain *B*. The distorted planar trigonal coordination of atoms O(3) (Fig. 4) involves Mg(2) atoms that lie off the local 2-fold axes of the *A* and *B* [Si–O(3)–Si] groups by  $32.7^\circ$  (*A*) and  $10.9^\circ$  (*B*) at Mg–O distances of 2.2881(7) Å and 2.4474(7) Å. In both groups, the longer Si–O bond lies nearer the Mg atom, and the greater difference of  $\Delta(\text{Si–O})$  in bond length occurs with the closer Mg approach distance. Such deformations suggest  $\text{Mg}^{2+} - \text{Si}^{4+}$  repulsion and

**Table 3.** Selected distances (Å) and angles (deg)<sup>a</sup> in orthoensstatite at 23 °C.

A. SiO <sub>4</sub> tetrahedra						
distance	Si(A)O <sub>4</sub>	Si(B)O <sub>4</sub>	O(i)–Si–O(j)		Si(A)O <sub>4</sub>	Si(B)O <sub>4</sub>
Si–O(i)			a	b		
a	1.6105	1.6185	a	b	107.98	107.34
b	1.6464	1.6775	a	c	112.66	106.23
c	1.6672	1.6751	a	d	117.18	117.22
d	1.5870	1.5877	b	c	105.30	111.11
	ave. 1.6278	1.6397	b	d	113.31	104.97
			c	d	99.68	109.98
					ave. 109.35	109.48
Si–O–Si bridge			e–O(b)–f		134.21	127.96
Symmetry operations on positions (Table 2) giving sites in Si(A)O <sub>4</sub> and Si(B)O <sub>4</sub>						
site	atom	operation				
a	O(1)	$x, y, z$				
b	O(3)	$x, y, z$				
c	O(3)	$x, \frac{1}{2} - y, \frac{1}{2} + z$				
d	O(2)	$x, y, z$				
e	Si	$x, y, z$				
f	Si	$x, \frac{1}{2} - y, -\frac{1}{2} + z$				
B. MgO <sub>6</sub> octahedra						
distance	Mg(1)O <sub>6</sub>	Mg(2)O <sub>6</sub>	angle		Mg(1)O <sub>6</sub>	Mg(2)O <sub>6</sub>
Mg–O(i)			O(i)–Mg–O(j)			
a	2.1516	2.0333	a	b	177.22	173.84
b	2.0469	1.9921	a	c	85.14	85.48
c	2.0657	2.4474	a	b	93.21	89.49
d	2.0279	2.0891	a	e	81.05	70.00
e	2.1709	2.2881	a	f	91.48	87.02
f	2.0087	2.0567	b	c	96.64	100.47
	ave. 2.0786	2.1511	b	d	84.93	84.73
			b	e	96.74	109.77
			b	f	90.74	94.62
			c	d	176.98	172.67
			c	e	91.69	75.36
			c	f	87.43	89.12
			e	f	172.52	152.92
			e	d	85.55	107.90
			f	d	95.15	85.29
Symmetry operation on positions (Table 2) giving sites in Mg(1)O <sub>6</sub> and Mg(2)O <sub>6</sub>						
Mg(1)O <sub>6</sub>			Mg(2)O <sub>6</sub>			
site	atom	operation	site	atom	operation	
a	O(1A)	$\frac{1}{2} - x, \frac{1}{2} + y, 1 + z$	a	O(2A)	$x, y, z$	
b	O(2B)	$x, y, z$	b	O(2B)	$x, y, z$	
c	O(1B)	$1 - x, 1 - y, 2 - z$	c	O(3B)	$x, \frac{1}{2} - y, -\frac{1}{2} + z$	
d	O(1A)	$\frac{1}{2} - x, 1 - y, \frac{1}{2} + z$	d	O(1A)	$\frac{1}{2} - x, 1 - y, \frac{1}{2} + z$	
e	O(1B)	$1 - x, \frac{1}{2} + y, \frac{1}{2} - z$	e	O(3A)	$x, \frac{1}{2} - y, \frac{1}{2} + z$	
f	O(2A)	$x, y, 1 + z$	f	O(1B)	$1 - x, 1 - y, 1 - z$	

<sup>a</sup> Estimated standard deviations are: Mg–O: 0.0007 Å; Si–O: 0.0008 Å; O–Mg–O: 0.03 °; O–Si–O: 0.04 °; Si–O–Si: 0.04 °.

consequent perturbation of the electron distributions in the bridging bonds by the Coulombic fields of  $\text{Mg}^{2+}$  ions at distances as great as 2.4 Å. Note that the difference between the *A*-chain bridging bonds, 0.031 Å, is as great as the average difference, 0.027 Å, between the two types of terminal bonds, Si–O(1) and Si–O(2), where O(1) is involved in a tetrahedral and O(2) in a trigonal pyramidal coordination (Fig. 4).

In the *A* and *B* tetrahedra, the terminal bonds differ by 0.023(1) Å and 0.031(1) Å, respectively, the shorter bonds, as expected, being those of 3-coordinated oxygen O(2) atoms, as opposed to the 4-coordinated oxygen O(1). The inter-chain differences in Si–O(1) and Si–O(2) bond lengths are not attributable to differences in asymmetry of local oxygen environments. The two Si–O(2) bond lengths are equal within 1  $\sigma$ , while the Si–O(1) bonds differ by 0.008 Å or 8  $\sigma$ . Yet, the O(1) coordinations are remarkably similar, while for O(2), there are marked differences in coordination angles Si–O(2)···Mg. Thus, the shorter and stronger terminal bonds appear to be less sensitive to local coordination differences than the longer bridging bonds.

In both chains, the largest O–Si–O angles, 117.18(3) and 117.22(3)°, are subtended by the two short, terminal Si–O bonds, while the smallest angles, 99.68(3)° and 104.97(3)°, are subtended by a bridging and a terminal bond. It should be noted that the unusually small angle of 99.68° in tetrahedron *A* involves the O(3)–O(2) edge, which is shared with the Mg(2) octahedron (Fig. 1).

The two Si–O(3)–Si angles are distinctly different [134.21(3)° in *A* and 127.96(3)° in *B*] and are both somewhat less than the average of 144° given for related silicates (Tossell and Gibbs, 1978). The wider angle goes with the shorter, bridging Si–O bonds, consistent with previous observations on the [Si–O–Si] bridging groups (see Gibbs, 1982) and quantum mechanical calculations on the  $\text{H}_6\text{Si}_2\text{O}_7$  molecule (Newton and Gibbs, 1980).

### The $\text{MgO}_6$ octahedra

The Mg(1) octahedra form the backbone of the zigzag double octahedral strip of  $\text{Mg}_2\text{O}_6$  extending along the *c* axis (Fig. 3). These octahedra are fairly regular with an average Mg–O distance of  $2.08 \pm 0.07$  Å and maximum angle distortion of 9.0°. On the other hand, the Mg(2) octahedra, which link the two tetrahedra–octahedra–tetrahedra (T–O–T) strips together are highly distorted (Figs. 2 and 3) with two unusually long bonds, Mg(2)–O(3A) = 2.2881(7) Å and Mg(2)–O(3B) = 2.4474(7) Å. In addition, the O(3A) bond angles are irregular, evidently as a result of the O(3A)···O(2A) edge-sharing with the *A* tetrahedron. The inequality of the two Mg(2)–O(3) bonds from each other is in contrast with the situation found in the high temperature *C*2/*c* phase of  $(\text{Mg,Fe})_2\text{Si}_2\text{O}_6$  (Smyth, 1974),

where these two bonds are equal. The present bonding situation is comparable to the effectively five-fold coordination of magnesium-rich M(4) polyhedron in ferromagnesian amphiboles, *viz.*, anthophyllite and primitive cummingtonite,  $(\text{Mg,Fe})_7\text{Si}_8\text{O}_{22}(\text{OH})_2$  (Ghose, 1982). It should be noted that these two long Mg(2)–O(3) bonds, particularly the longer one, are very sensitive to temperature, pressure and chemical substitution (Smyth, 1973; Ralph and Ghose, 1980; Ghose, 1982). Thus, a precise determination of these bond length values in enstatite is important for estimating the amount of substituting cations, such as Al in aluminous orthopyroxenes, which cannot be easily distinguished from Mg by X-ray diffraction (Ganguly and Ghose, 1979).

#### Anisotropic thermal motion

The nuclear  $U_{ij}$  parameters provide a realistic pattern of r.m.s. displacements (mainly thermal vibrations) consistent with the bonding environments in the crystal. For chemically equivalent atoms of the two silicate chains, the r.m.s. amplitudes of vibration along respective principal axes of the thermal ellipsoids (Table 4A) are equal within  $2\sigma$ , except for bridging atoms O(3A) and O(3B), which have distinctly different bonding environments. As expected, atoms O(2) and O(3), in trigonal sites, show greater thermal anisotropy than do atoms Si and O(1), with their more nearly isotropic tetrahedral configurations. Likewise, the anisotropy and amplitudes of vibration are greater for Mg(2), in the more distorted and larger octahedron, than for Mg(1). In the silicate chains, the r.m.s. displacements of Si and O along respective Si–O bonds (Table 4B) are nearly equal, in accord with the great strength of these bonds. (This correlated motion is a necessary, but not a sufficient, condition that the  $[\text{SiO}_4]$  tetrahedra vibrate as rigid groups.) The vibrational motion of adjacent Mg and O atoms also appear to be coupled in the  $[\text{Mg}(1)\text{O}_6]$  group, though to a lesser extent, and, to a much lesser extent in the larger  $[\text{Mg}(2)\text{O}_6]$  group.

In the following discussion, we present a rigid-body analysis of the thermal vibrations of the two distinct silicate tetrahedra with attempts to account for their internal vibrations. This analysis is not concerned with correlations between the motion of a particular  $[\text{SiO}_4]$  group and the atoms of the rest of the crystal, nor does it account for the forces involved, e.g., the Coulombic interaction with the  $\text{Mg}^{2+}$  ions.

#### Rigid-body analysis of the thermal vibration of the silicate tetrahedra and the thermal correction of the Si–O bond lengths

In a silicate such as enstatite, the interatomic forces within a tetrahedral  $[\text{SiO}_4]$  group are much stronger than the forces between such groups (except, of course, for the forces that link the tetrahedra into chains). In any

case, if there is appreciable vibration, bond lengths may require correction: the distance between the average positions of two atoms on a crystal structure, as found by diffraction, is shorter than the average distance between these atoms to an extent that depends on the mean square *relative transverse* displacements of the atoms (Cruickshank, 1956; Busing and Levy, 1964). These relative displacements are not fully defined by the

**Table 4.** Amplitude and directions of nuclear thermal motion at 23°C.

A. R.m.s. displacements and orientations of principal axes of thermal ellipsoids relative to crystal axes *a*, *b*, *c*

Atom	Principal axes	R.m.s.d.	Angles with crystal axes <sup>a</sup>		
			<i>a</i>	<i>b</i>	<i>c</i>
Mg(1)	1	0.060(1) Å	78(3)°	92(9)°	13(3)°
	2	0.067(1)	101(5)	169(5)	90(9)
	3	0.080(1)	16(4)	101(4)	105(3)
Mg(2)	1	0.066(1)	65(2)	94(4)	25(2)
	2	0.080(1)	107(3)	163(3)	86(4)
	3	0.097(1)	31(2)	107(3)	115(2)
Si(A)	1	0.051(2)	105(11)	91(13)	15(11)
	2	0.057(2)	128(10)	140(8)	100(16)
	3	0.066(2)	42(8)	130(8)	79(6)
Si(B)	1	0.052(2)	72(8)	128(15)	43(16)
	2	0.057(2)	80(13)	136(16)	133(16)
	3	0.064(2)	21(9)	70(11)	97(11)
O(1A)	1	0.062(1)	7(5)	84(4)	94(7)
	2	0.069(1)	93(7)	105(10)	164(10)
	3	0.075(1)	97(4)	17(10)	105(10)
O(1B)	1	0.064(1)	35(15)	98(6)	57(15)
	2	0.068(1)	125(15)	101(7)	37(15)
	3	0.075(1)	90(6)	14(6)	76(6)
O(2A)	1	0.060(1)	61(2)	29(2)	92(5)
	2	0.072(1)	109(3)	82(5)	160(2)
	3	0.095(1)	35(2)	117(1)	110(2)
O(2B)	1	0.057(1)	58(1)	135(3)	62(4)
	2	0.072(1)	85(3)	120(3)	150(4)
	3	0.095(1)	32(1)	60(2)	101(2)
O(3A)	1	0.058(1)	87(4)	65(2)	26(2)
	2	0.074(1)	167(3)	77(3)	93(3)
	3	0.093(1)	77(2)	29(2)	115(1)
O(3B)	1	0.059(1)	93(4)	63(3)	28(2)
	2	0.073(1)	151(3)	116(4)	80(4)
	3	0.087(1)	62(3)	140(3)	65(2)

